Supplemental Information

Cryo-EM Structure of Caspase-8 Tandem DED Filament Reveals Assembly and Regulation Mechanisms of the Death Inducing Signaling Complex

Tian-Min Fu, Yang Li, Alvin Lu, Zongli Li, Parimala R. Vajjhala, Anthony C. Cruz, Devendra B. Srivastava, Frank DiMaio, Pawel A. Penczek, Richard M. Siegel, Katryn J. Stacey, Edward H. Egelman and Hao Wu

Inventory of Supplemental Information

SUPPLEMENTAL FIGURES

SUPPLEMENTAL EXPERIMENTAL PROCEDURES

SUPPLEMENTAL REFERENCES

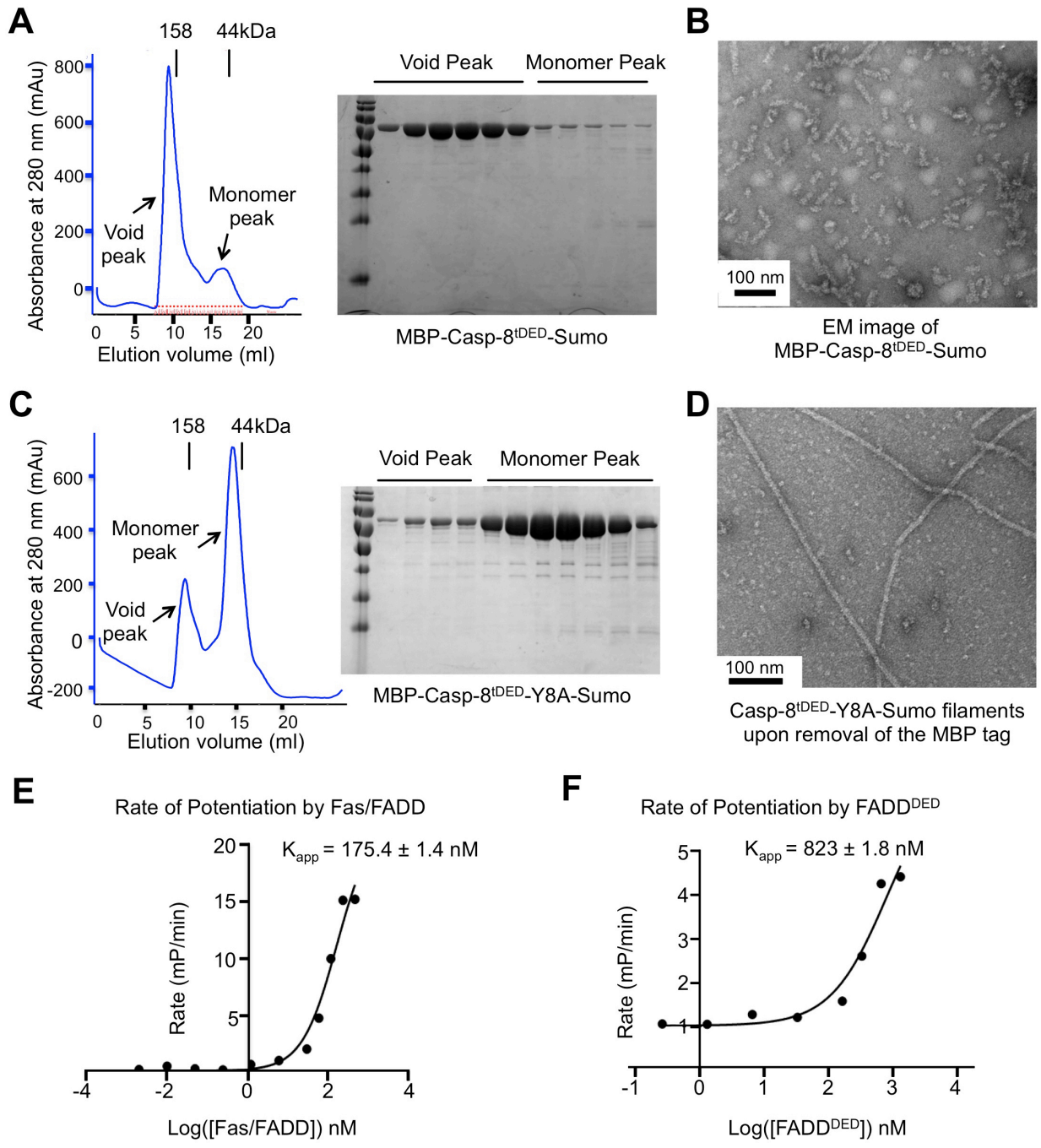

Figure S1. The Fas/FADD Complex, FADD^{DED} and ASC^{PYD} Promote Casp-8^{tDED} Filament Formation, Related to Figure 1

(A) Gel filtration profile and SDS-PAGE of MBP-Casp-8^{tDED}-Sumo.
(B) An electron micrograph of MBP-Casp-8^{tDED}-Sumo short filaments.
(C) Gel filtration profile and SDS-PAGE of MBP-Casp-8^{tDED}-Y8A-Sumo.
(D) An electron micrograph of Casp-8^{tDED}-Y8A-Sumo filaments upon removal of the MBP tag.

(E) Calculated K_{app}, with fitting error, for Fas/FADD-mediated potentiation of Casp-8^{tDED} polymerization.
(F) Calculated K_{app}, with fitting error, for $FADD^{DED}$-mediated potentiation of Casp-8^{tDED} polymerization.

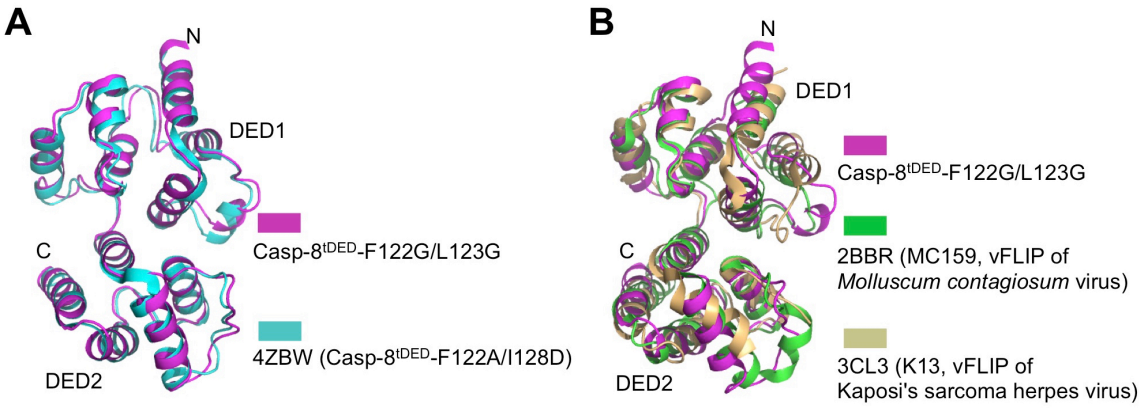
A
N
DED1
C
DED2
Casp-8tDED-F122G/L123G
4ZBW (Casp-8tDED-F122A/I128D)
B
N
DED1
C
DED2
Casp-8tDED-F122G/L123G
2BBR (MC159, vFLIP of Molluscum contagiosum virus)
3CL3 (K13, vFLIP of Kaposi's sarcoma herpes virus)

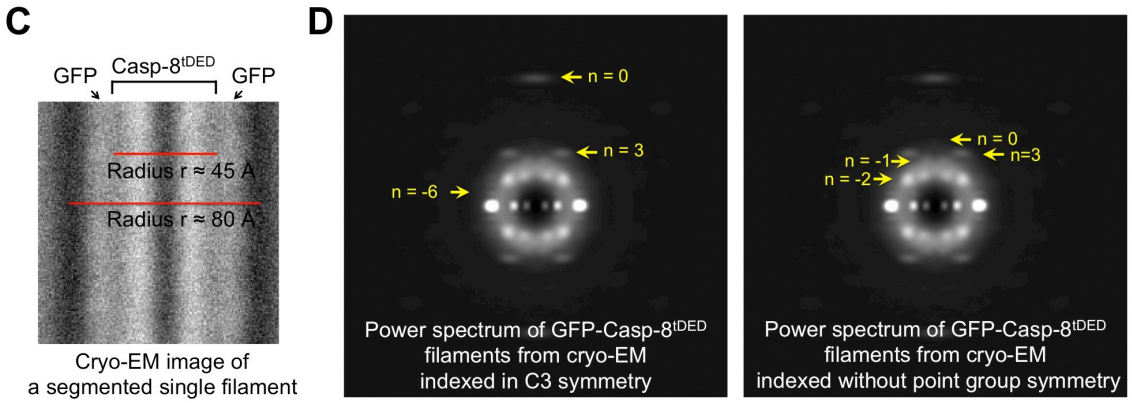
C
GFP
Casp-8tDED
GFP
Radius r ≈ 45 Å
Radius r ≈ 80 Å
Cryo-EM image of a segmented single filament
D
n = 0
n = 3
n = -6
Power spectrum of GFP-Casp-8tDED filaments from cryo-EM indexed in C3 symmetry
n = 0
n=3
n = -1
n = -2
Power spectrum of GFP-Casp-8tDED filaments from cryo-EM indexed without point group symmetry

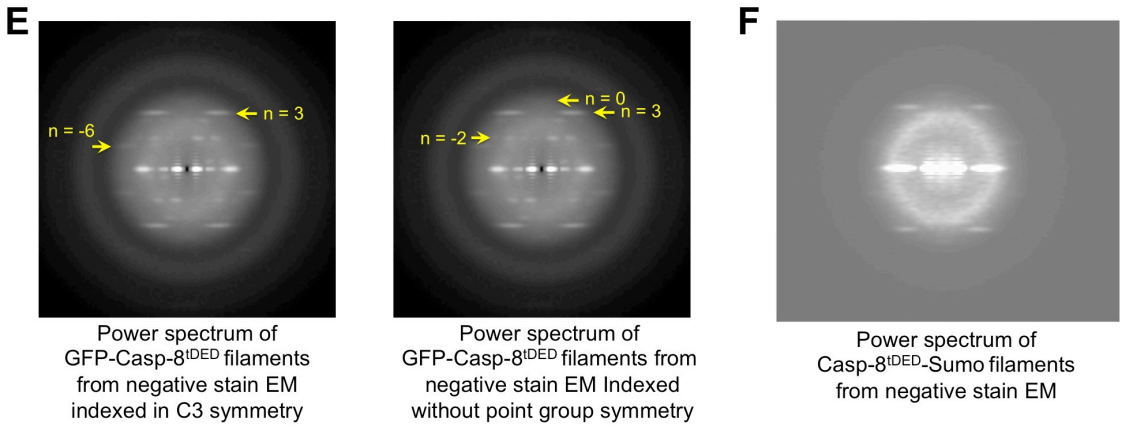
E
n = -6
n = 3
Power spectrum of GFP-Casp-8tDED filaments from negative stain EM indexed in C3 symmetry
n = 0
n = 3
n = -2
Power spectrum of GFP-Casp-8tDED filaments from negative stain EM Indexed without point group symmetry
F
Power spectrum of Casp-8tDED-Sumo filaments from negative stain EM

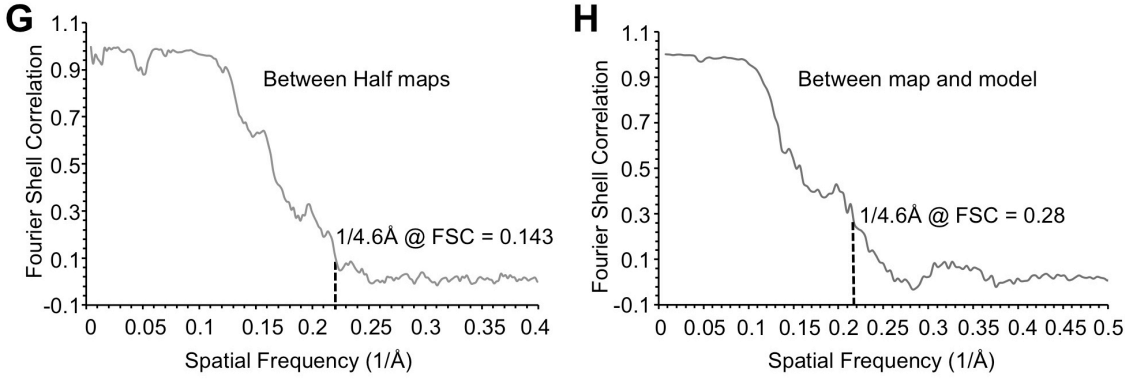
G
Fourier Shell Correlation
1.1
0.9
0.7
0.5
0.3
0.1
-0.1
Between Half maps
1/4.6Å @ FSC = 0.143
0 0.05 0.1 0.15 0.2 0.25 0.3 0.35 0.4
Spatial Frequency (1/Å)
H
Fourier Shell Correlation
1.1
0.9
0.7
0.5
0.3
0.1
-0.1
Between map and model
1/4.6Å @ FSC = 0.28
0 0.05 0.1 0.15 0.2 0.25 0.3 0.35 0.4 0.45 0.5
Spatial Frequency (1/Å)

Figure S2. Crystal Structure of MBP-Casp-8^{tDED}-F122G/L123G and Cryo-EM Reconstruction of the GFP-Casp-8^{tDED} Filament, Related to Figure 2

(A) Structural superposition of Casp-8^{tDED}-F122G/L123G (magenta) with the published Casp-8^{tDED} structure (cyan, PDB 4ZBW).

(B) Structural superposition of Casp-8^{tDED}-F122G/L123G (magenta) with the vFLIP of Molluscum contagiosum virus MC159 (green, PDB 2BBR) and the vFLIP of Kaposi's sarcoma herpes virus ks-vFLIP (cyan, 3CL3).

(C) The measured radii of GFP-Casp-8^{tDED} filaments, with or without the outer layer of GFP.

(D) Power spectra calculated from cryo-EM images of GFP-Casp-8^{tDED} filaments, labeled with the indices of a few observed layer lines for C3 symmetry and without point group symmetry.

(E) Power spectra calculated from negative staining EM images of GFP-Casp-8^{tDED} filaments, labeled with the indices of a few observed layer lines for C3 symmetry and without point group symmetry.

(F) Power spectrum calculated from negative staining EM images of Casp-8^{tDED}-Sumo filaments.

(G) Fourier shell correlation (FSC) plot between independently reconstructed half maps. The nominal resolution is 4.6 Å at FSC=0.143.

(H) FSC plot between the final cryo-EM map and the final model.

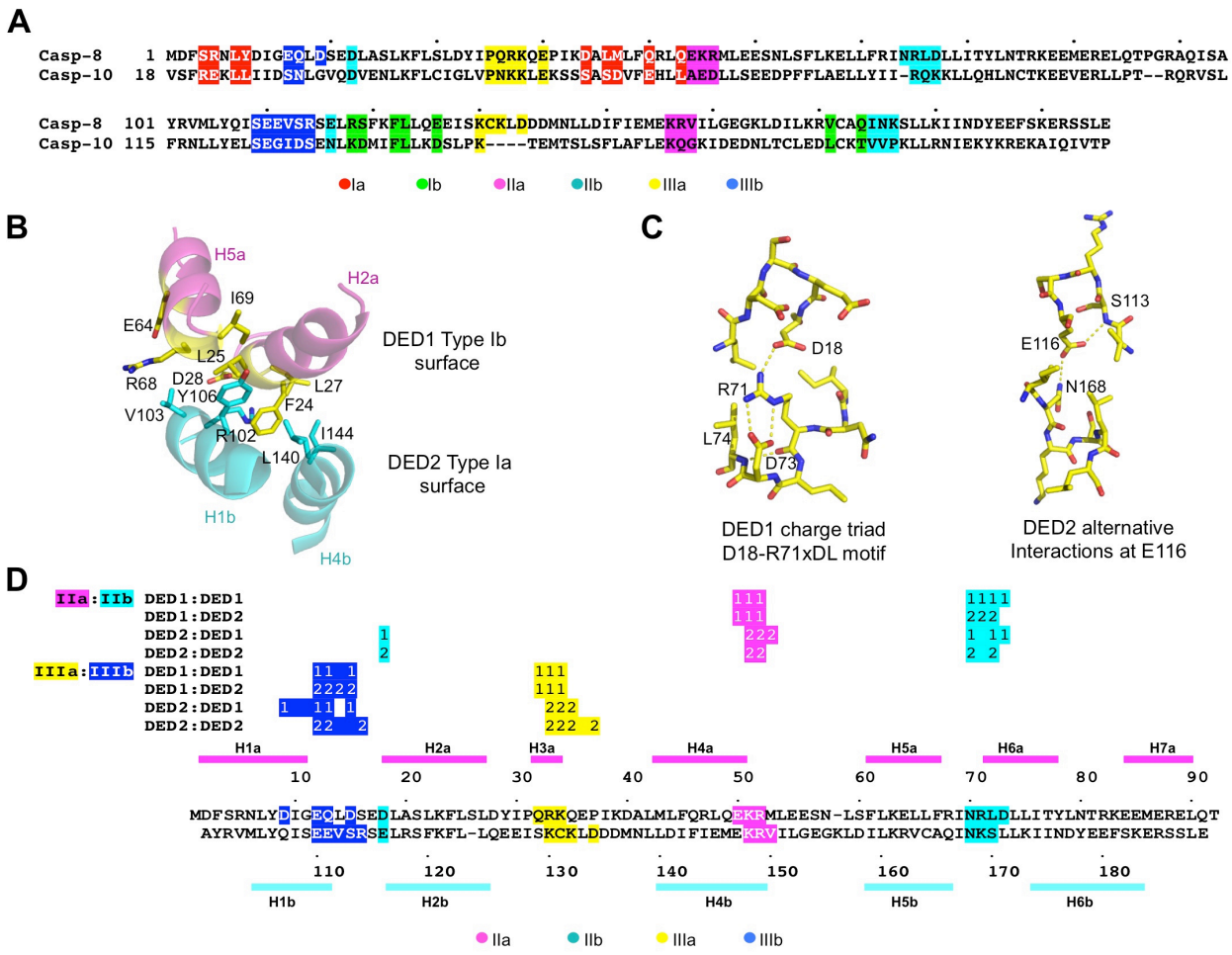

Figure S3. Interactions between DED1 and DED2 and Quasi-Equivalent Interactions in the Casp-8^{tDED} Filament, Related to Figure 3

(A) Sequence alignment of Casp-8^{tDED} and Casp-10^{tDED}, showing the similarity of the key residues on three interfaces, colored with type Ia in red, type Ib in green, type IIa in magenta, type IIb in cyan, type IIIa in yellow and type IIIb in blue.

(B) Detailed interactions between DED1 and DED2 in the Casp-8^{tDED} crystal structure.

(C) Stick model for the interactions in the charge triad of DED1 and DED2.

(D) Sequence alignment of Casp-8 DED1 and DED2, showing the locations of the four quasi-equivalent type II and type III interactions, highlighted with type IIa in magenta, type IIb in cyan, type IIIa in yellow and type IIIb in blue.

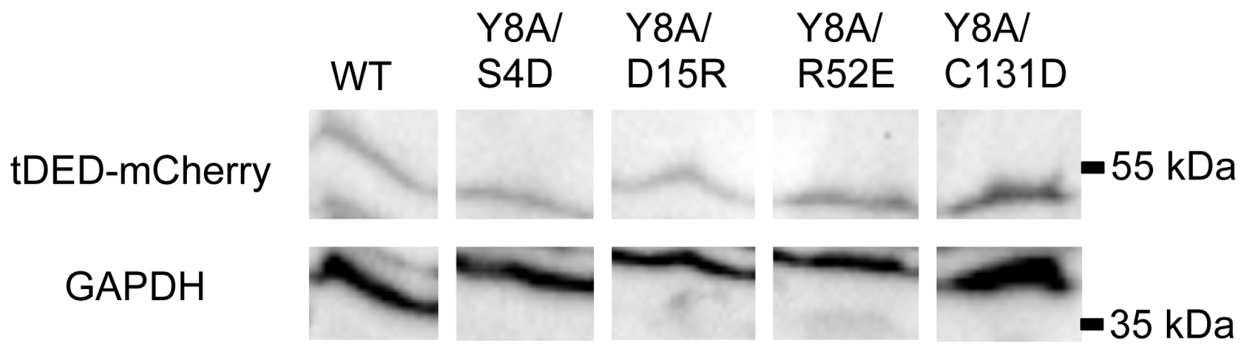

Figure S4. Western blot analysis for the expression of WT and mutant Casp-8-mCherry in HeLa cells, Related to Figure 4

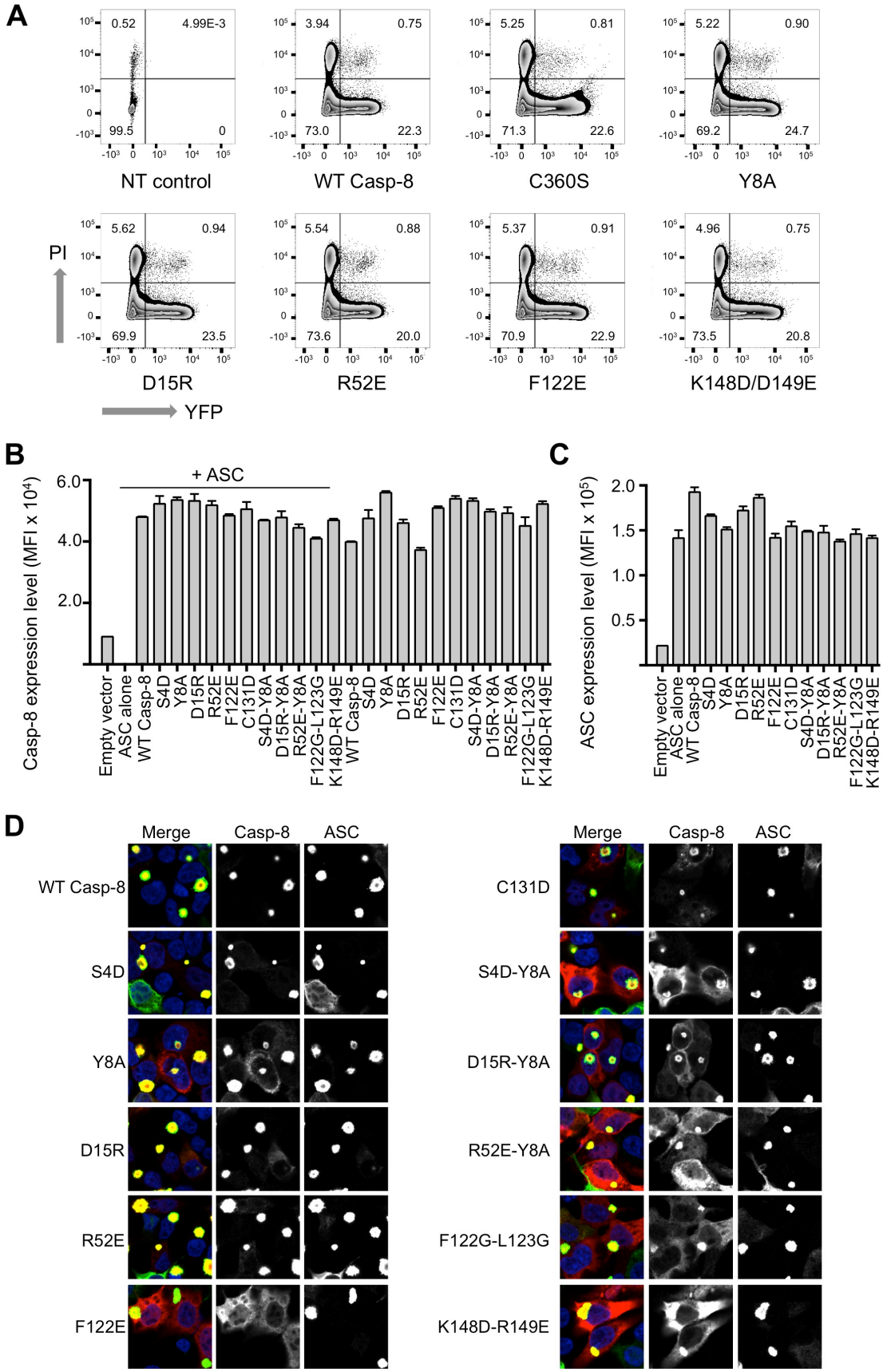
A
0.52
4.99E-3
99.5
0
NT control
3.94
0.75
73.0
22.3
WT Casp-8
5.25
0.81
71.3
22.6
C360S
5.22
0.90
69.2
24.7
Y8A
5.62
0.94
69.9
23.5
D15R
5.54
0.88
73.6
20.0
R52E
5.37
0.91
70.9
22.9
F122E
4.96
0.75
73.5
20.8
K148D/D149E
PI
YFP
B
+ ASC
Casp-8 expression level (MFI x 10⁴)
6.0
4.0
2.0
Empty vector
ASC alone
WT Casp-8
S4D
Y8A
D15R
R52E
F122E
C131D
S4D-Y8A
D15R-Y8A
R52E-Y8A
F122G-L123G
K148D-R149E
C
ASC expression level (MFI x 10⁵)
2.0
1.5
1.0
0.5
D
Merge
Casp-8
ASC
WT Casp-8
S4D
Y8A
D15R
R52E
F122E
C131D
S4D-Y8A
D15R-Y8A
R52E-Y8A
F122G-L123G
K148D-R149E

Figure S5. Filament Formation-Defective Mutants of Casp-8 Compromised Death Receptor- and Inflammasome-Mediated Signaling, Related to Figure 5

(A) Expression of WT and mutant Casp-8 in I9.2C and the spontaneous cell death. Casp-8 deficient I9.2C cells were transfected with WT and mutant Casp-8 fused with YFP. The expression level and cell death by propidium Iodide (PI) staining were accessed by flow cytometry.

(B) WT and mutant Casp-8 expression levels with and without co-transfection of ASC. Mean and range of duplicate transfections in a representative experiment are shown.

(C) ASC expression levels with and without co-transfection of WT and mutant Casp-8. Mean and range of duplicate transfections in a representative experiment are shown.

(D) Specks formed by Casp-8 variants and ASC in HEK293T cells. HEK293T cells were transfected with plasmids expressing ASC and Myc-tagged Casp-8. All Casp-8 constructs contain the C360S mutation in addition to the stated mutations. ASC was detected using an anti-ASC antibody (green) while Casp-8 was detected using an anti-Myc antibody (red) and nuclei were stained with DAPI.

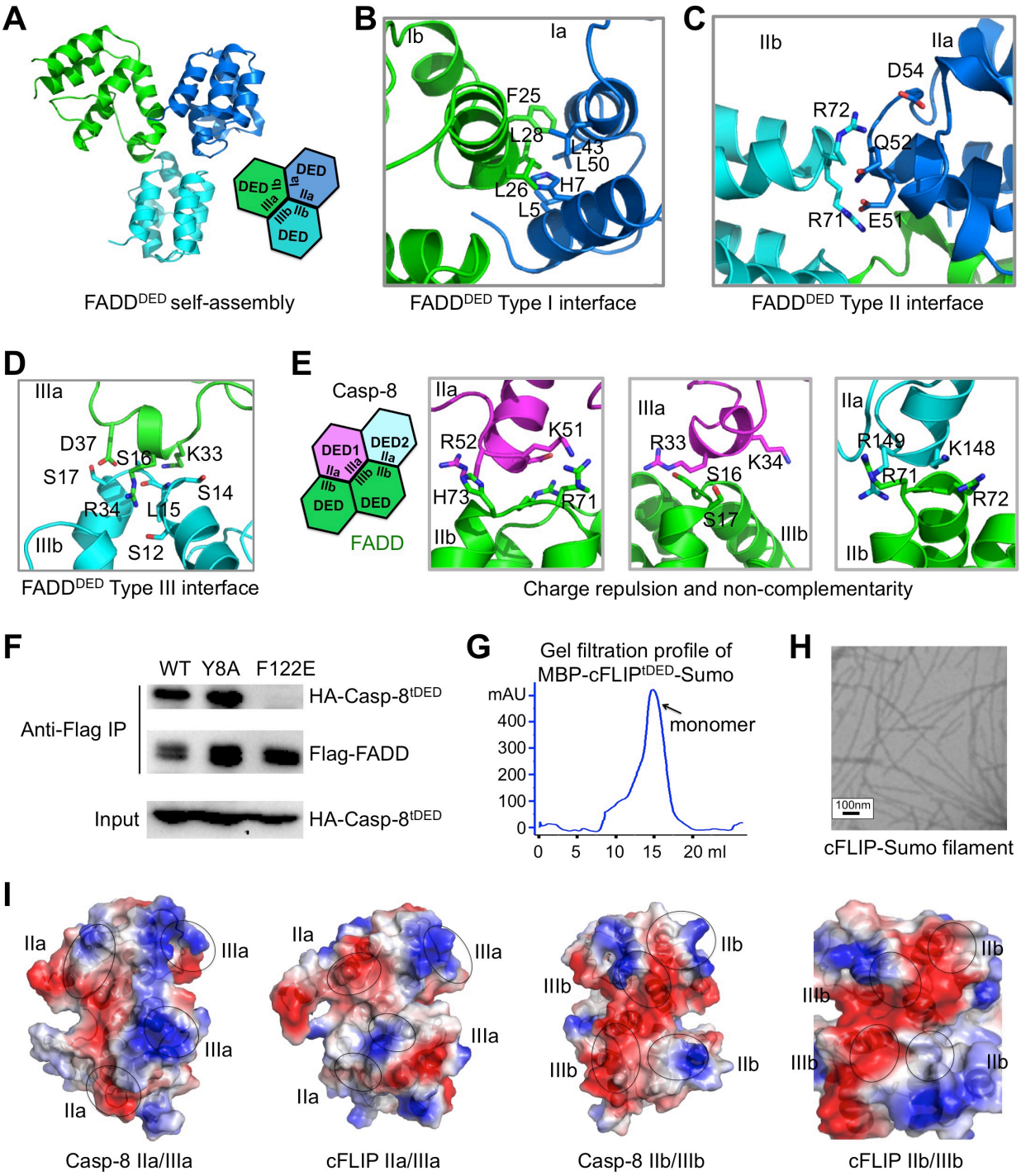

Figure S6. Insights into DED/DED interactions among FADD^{DED}, Casp-8^{tDED} and cFLIP^{tDED}, Related to Figure 6

(A) Model of FADD^{DED} self-assembly showing the three types of interactions.

(B) The predicted type I interface in the FADD^{DED} filament, showing the hydrophobic nature of the surfaces.

(C, D) The predicted type II (C) and type III (D) interfaces in the FADD^{DED} filament, showing the hydrophilic and charged surfaces.

(E) Charge repulsion and non-complementarity in the type II and type III interactions between FADD and Casp-8 when the molecules are swapped from what are predicted in Figure 6D.
(F) Lack of effect of the Y8A Casp-8 mutation and disruption by the F122E Casp-8 mutation in the FADD/Casp-8 interaction. Flag-FADD was co-expressed in HEK293T cells with WT and mutant HA-Casp-8^{tDED}, immunoprecipitated with anti-Flag, and immunoblotted with anti-HA and anti-Flag.
(G) Gel filtration profile and SDS-PAGE showing that MBP-cFLIP^{tDED}-Sumo eluted as monomer.
(H) MBP-cFLIP^{tDED}-Sumo formed filament upon removal of the MBP tag.
(I) Comparison of the electrostatic interfaces of cFLIP^{tDED} and Casp-8^{tDED}.

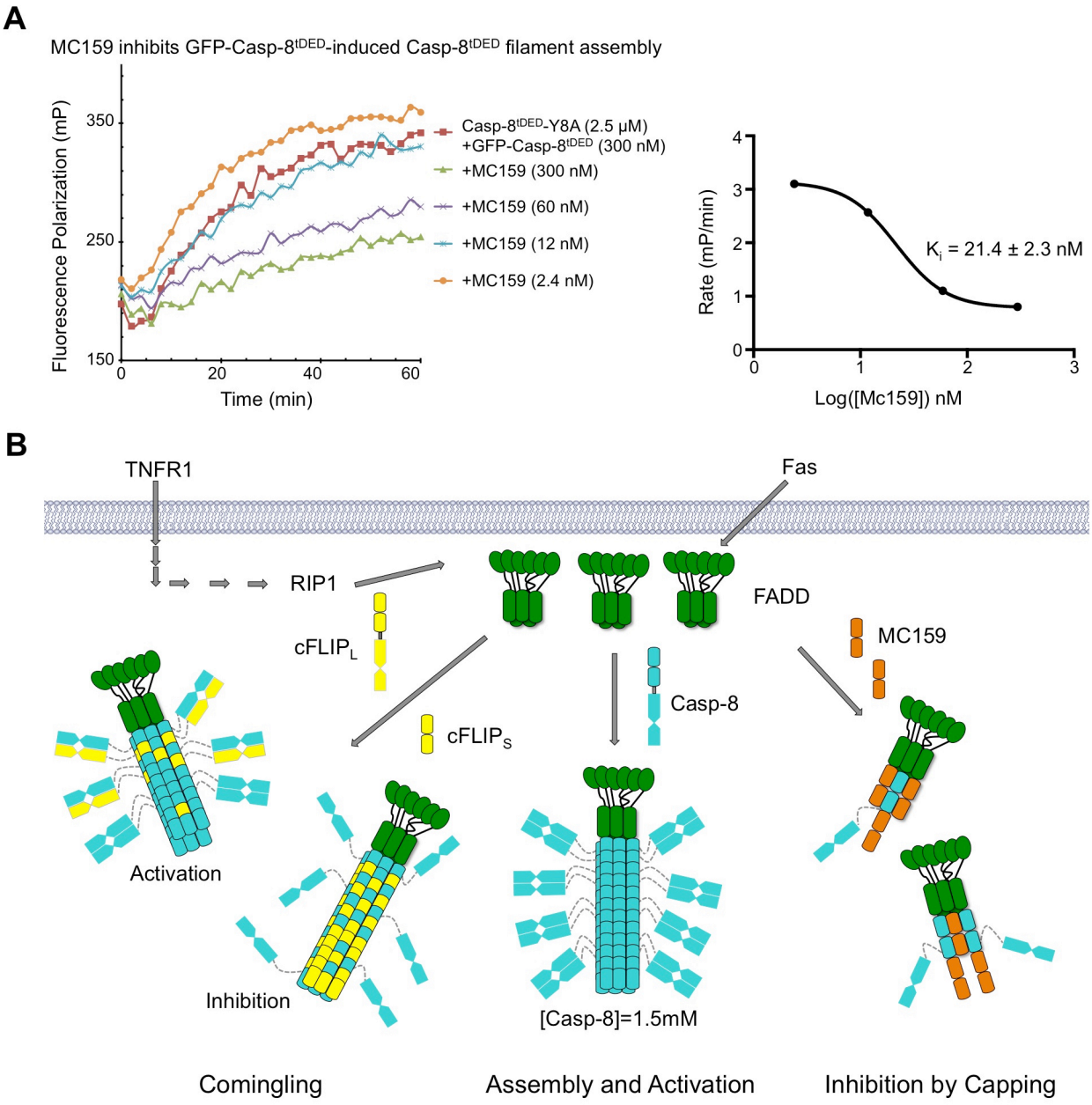

Figure S7. Assembly and regulation of Casp-8 at the DISC, Related to Figure 7

(A) Inhibition of GFP-Casp8^{tDED}-induced Casp-8^{tDED} polymerization by MC159. Calculated K_i, with fitting error, is shown.

(B) A schematic model of Casp-8 assembly and regulation upon death receptor ligation.

SUPPLEMENTAL EXPERIMENTAL PROCEDURES

Casp-8^{tDED} Filament, FADD^{DED} Filament, and cFLIP Filament Preparation

The tDED domain of human Casp-8 and the DED domain of FADD were cloned into a pET28a vector containing the monomeric, A206K mutant of GFP to generate constructs with non-cleavable N-terminal 6xHis-GFP-tags. The constructs were transformed into *E. coli* BL21(DE3) cells for IPTG inducible expression. These cells were lysed by sonication in a lysis buffer containing 20 mM HEPES at pH 8.0, 200 mM NaCl, 15 mM imidazole. The cell lysate was incubated with Ni-NTA resin for half hour. The resins were washed with lysis buffer containing 20 mM imidazole, and target proteins were eluted with lysis buffer containing 300 mM imidazole. The Ni-NTA eluates were injected onto a Superdex 200 column, and the void fractions containing GFP-Casp-8^{tDED} or GFP-FADD^{DED} filaments were used for EM studies. The cFLIP^{tDED} was cloned into a pDB-His-MBP vector and expressed in *E. coli*. The protein was similarly purified by Ni-affinity and gel filtration chromatography. The void fraction was collected and digested by the tobacco etch virus (TEV) protease for 4 hours to remove the His-MBP tag. After TEV cleavage, the sample was used for EM study.

Crystallization and Data Collection of Casp-8^{tDED}

The tandem DED of Casp-8 (residues 1-186) was cloned into the pDB-His-MBP vector. In order to obtain monomeric Casp-8, residues F122 and L123 were both mutated to Gly through site-directed mutagenesis. The protein was purified by Ni-affinity and gel filtration chromatography. The purified protein was concentrated to 30 mg/ml for crystallization experiments at 293K using hanging drop vapor diffusion. The best crystals were obtained with a reservoir condition of 0.1 M MMT (DL-malic acid, MES, Tris in molar ratio of 1:2:2) at pH 8.0 and 25% PEG1500.

Crystal Structure Determination of MBP-Casp-8^{tDED}

Diffraction data were collected at beam line 24ID-E, Advanced Photon Source (APS) and processed using HKL2000 (Otwinowski and Minor, 1997). Initial phases for the MBP-Casp-8^{tDED} crystal diffraction data were first obtained by molecular replacement calculations in Phaser (McCoy et al., 2007) using the MBP structure (PDB ID, 3VD8) as a template. Iterative model building in Coot (Emsley and Cowtan, 2004) and structure refinement in Phenix.refine (Adams et al., 2010) resulted in a complete atomic model of Casp-8^{tDED}. Structural representations were displayed using Pymol (Delano, 2002).

Electron Microscopy (EM) Data Collection

To assess the quality of Casp-8^{tDED} filaments, they were negatively stained as described (Ohi et al., 2004) and examined on a CM10 electron microscope (Philips) operated at an acceleration voltage of 100 kV. Data collection of negatively stained specimen was performed on a Tecain T12 microscope (FEI) operated at an acceleration voltage of 120 kV using FEI standard room temperature holder (FEI). Images were recorded on the Gatan US4000 CCD camera (Gatan) at the nominal magnification of 42,000x, which corresponds to a calibrated magnification of 57,555x on the image plane of the CCD camera.

For cryo-EM, 3.5 µL 0.2 mg/ml GFP-Casp-8^{tDED} sample was applied to glow-discharged Quantifoil R1.2/1.3 holy carbon grids (Quantifoil, Germany) and plunge-frozen using a Vitrobot Mark I (FEI). Data collection was performed on a Tecnai F20 electron microscope (FEI) operated at an acceleration voltage of 200 kV using a CT3500 cryo-specimen holder (Gatan) and the UCSF Image4 software (Li et al., 2013). Micrographs were recorded in movie mode at liquid nitrogen temperature with a K2 Summit direct electron detection camera (Gatan) operated in super-resolution mode with dose-fractionation. The nominal magnification was 29,000x, which corresponds to a calibrated magnification of 40,410x on the sensor plane of the camera. The beam intensity was set to be 8 electrons/pixel/second. During a 6-second exposure, 30 200-ms

frames were collected, resulting in a total electron dose of 31 electrons/Å^2. The frames were binned over 2 x 2 pixels, yielding a pixel size of 1.24 Å, and aligned to each other using the program MotionCorr (Li et al., 2013). After motion correction, the frames were summed up and used for further image processing.

Cryo-EM Image Processing and Model Refinement

A total of 388 images were used for analysis and processing. The contrast transfer function (CTF) of each image was determined using CTFFIND3 (Mindell and Grigorieff, 2003). The SPIDER software package (Frank et al., 1996) was used for most subsequent processing. Images were first multiplied (in reciprocal space) by respective CTFs and then filaments were boxed using the e2helixboxer routine within EMAN2 (Tang et al., 2007). Overlapping boxes of 384 px in dimensions (1.24 Å/px) were cut from the long filament boxes, using a shift of 32 px between adjacent boxes (92% overlap). Helical averaging was performed using the iterative helical real space reconstruction (IHRSR) algorithm (Egelman, 2010).

Initial calculations used a C3 symmetry with ~53° right-handed rotation and ~14.0 Å axial rise per subunit, as determined from the power spectra, and yielded a reconstruction with recognizable secondary structures. However, the asymmetric unit of the C3 symmetry can only accommodate a single DED, and because DED1 and DED2 were considered the same, the connecting helix (H7a) between the domains was averaged out (Figure 2H). Removing the C3 symmetry and using a rotation of 99.4° and an axial rise of 27.1 Å for three complete tDED molecules resulted in the correct connection between DED1 and DED2, as well as matching the observed power spectrum which could not be explained by the C3 symmetry. A total of 33,969 segments were used in the final reconstruction. The Casp-8^{tDED} crystal structure was fit into the cryo-EM density using UCSF Chimera (Pettersen et al., 2004) and refined in real space using Rosetta (DiMaio et al., 2015). The final cryo-EM model remains highly similar to the crystal structure with RMSD of 0.98 Å.

Modeling of Other DED Filament Structures Based on the Casp-8^{tDED} filament Structure

The monomeric cFLIP^{tDED} structure model was generated by SWISS-MODEL (Biasini et al., 2014) using the MC159 crystal structure (PDB ID 2BBR) as a template. FADD^{DED} structure (PDB ID 2GF5) and cFLIP^{tDED} model were superimposed onto Casp-8^{tDED} filament structure in Coot (Emsley and Cowtan, 2004) to generate the filament models, which were then subjected to minimization using Phenix.geometry-minimization (Adams et al., 2010). The clash scores from MolProbity (Chen et al., 2010) are 6.8 and 7.7 for FADD^{DED} and cFLIP^{tDED} filaments, respectively. The superimposed RMSD between the cFLIP^{tDED} model and Casp-8^{tDED} is 1.6 Å. FADD^{DED} shows RMSD values of 1.9 Å and 1.7 Å with Casp-8^{DED1} and Casp-8^{DED2}, respectively.

Western Blot to Assess the Expression of Casp-8^{tDED}-mCherry Wild Type and Mutants

The wild type and mutant Casp-8^{tDED}-mCherry were transfected into HeLa cells according to stand protocol. One day post transfection, the cells were lysed and centrifuged to remove cell debris. The supernatant was used for western blotting. The Casp-8^{tDED}-mCherry was detected by anti-mCherry antibody (Abcam).

Sortase Labeling and Fluorescence Polarization (FP) Assay

MBP-tagged Casp-8^{tDED}-Sumo remained an aggregate that eluded in the void fraction of a Superdex 200 column. In order to obtain monomeric Casp-8^{tDED} suitable for FP assay, we searched for a partially defective mutant with the ability to polymerize. MBP-tagged Casp-8^{tDED}-Sumo with the Y8A mutation eluted in the monomeric position of a Superdex200 column, and cleavage of the MBP tag generated individual filaments. We also added a “LPETGG” sequence at the C-terminus for sortase labeling (Guimaraes et al., 2013). This construct was expressed in *E. coli* BL21(DE3). The fusion protein was purified using Ni-NTA resin and Superdex 200

column as a monomer. It was then labeled through a sortase reaction using 5 μM calcium-independent sortase, 30 μM substrate (MBP-Casp-8^{tDED}-Y8A-Sumo), and 500 μM nucleophile containing the fluorophore (GGG-TAMRA). The mixture was incubated on ice overnight and passed through a Superdex 200 column. FP readings were taken on a SpectraMax M5e (Molecular Devices) using excitation and emission wavelengths of 561 nm and 585 nm. The same procedure was used for the cFLIP FP assay using the His-MBP-cFLIP-Sumo construct.

Cell Death Assay Induced by Fas Ligand (FasL)

Wild type and mutant Casp-8 constructs were cloned into the pcDNA3.1-YFP vector for subsequent cell death assays. 8x10^6 Casp-8 deficient Jurkat cells (clone I9.2) were transfected with 25 μg plasmid DNA of WT or mutant Casp-8 via electroporation (BTX ECM 830, Harvard Apparatus). 24 hrs post-transfection, cells were treated with increasing amounts of FasL fused to an isoleucine zipper (FasL-LZ) for 8 hrs at 37 °C. YFP$^+$ cells were analyzed for cell death via Annexin V and Live/Dead staining (Invitrogen) as previously described (Ramaswamy et al., 2011).

Recruitment of Caspase-8 to ASC Specks Using Flow Cytometry

A catalytically inactive Casp-8 mutant, which contains a cysteine to serine mutation in the active site (C360S), was PCR amplified with a C-terminal Myc-tag and cloned into pcDNA3.1(+). Individual mutations (S4D, Y8A, D15R, R52E, F122E, C131D) and double mutations (S4D/Y8A, D15R/Y8A, R52E/Y8A, F122G/L123G, K148D/R149E) in the tandem DEDs were introduced into the Casp-8 C360S mutant plasmid using the QuikChange mutagenesis protocol. pcDNA-ASC was a gift from Dr. Naohiro Inohara. The assay was performed as described previously (Sester et al., 2016). The immunostained cells were analyzed on a BD Accuri C6 equipped with a 488 nm laser and 530/30 nm, 585/40 nm and 670 nm LongPass filters. Data was analyzed for changes in the ratio of fluorescence peak height to area, indicating movement of ASC and Casp-8 from diffuse to speck localization.

Imaging the Recruitment of Caspase-8 to ASC Specks by Fluorescence Microscopy

HEK293T cells (100,000) were seeded in 24-well dishes on coverslips coated with poly-L-lysine (Sigma). For transfection, 200 ng of pcDNA-ASC was combined with 50 ng of plasmid expressing wild-type or mutant Casp-8 and 150 ng of empty vector. Lipofectamine was added at a 2.5:1 (ml: mg) ratio of lipofectamine to DNA. Cells were incubated overnight (~18 h), and fixed with 4% paraformaldehyde prepared in PBS for 15 min. Cells were then permeabilised and blocked in PBS containing 10% FCS, 0.3% saponin, 0.1% sodium azide for 45 min. Myc-tagged Casp-8 was detected using mouse monoclonal (9B11) anti-Myc antibody (Cell Signaling Technology) followed by goat anti-mouse–Alexa Fluor-555 (Life Technologies). ASC was detected using rabbit polyclonal anti-ASC (N-15) (Santa Cruz Biotechnology) followed by goat anti-rabbit–Alexa Fluor-488 (Life Technologies). All antibodies were diluted 1:1000 in PBS containing 2% FCS, 0.06% saponin and 0.02% sodium azide. Primary antibodies were incubated for 2 h at room temperature while secondary antibodies were incubated for 1 h at room temperature. Unbound antibodies were washed away using PBS containing 0.04% Tween-20. 4',6-diamidino-2-phenylindole (DAPI) was added to the secondary antibody at a final concentration of 2 mg/ml. Coverslips were mounted on slides with fluorescent mounting medium (Dako). Microscopy was performed using a Zeiss LSM 710 laser scanning confocal microscope using Zeiss Zen software and captured under identical settings. Images from the LSM 710 were merged using ImageJ.

SUPPLEMENTAL REFERENCES

Adams, P.D., Afonine, P.V., Bunkoczi, G., Chen, V.B., Davis, I.W., Echols, N., Headd, J.J., Hung, L.W., Kapral, G.J., Grosse-Kunstleve, R.W.*, et al.* (2010). PHENIX: a comprehensive Python-based system for macromolecular structure solution. Acta Crystallogr D Biol Crystallogr *66*, 213-221.

Biasini, M., Bienert, S., Waterhouse, A., Arnold, K., Studer, G., Schmidt, T., Kiefer, F., Cassarino, T.G., Bertoni, M., Bordoli, L.*, et al.* (2014). SWISS-MODEL: modelling protein tertiary and quaternary structure using evolutionary information. Nucleic Acids Res *42*, W252-258.

Chen, V.B., Arendall, W.B., 3rd, Headd, J.J., Keedy, D.A., Immormino, R.M., Kapral, G.J., Murray, L.W., Richardson, J.S., and Richardson, D.C. (2010). MolProbity: all-atom structure validation for macromolecular crystallography. Acta Crystallogr D Biol Crystallogr *66*, 12-21.

Delano, W.L. (2002). The PyMol Molecular Graphics System.

DiMaio, F., Song, Y., Li, X., Brunner, M.J., Xu, C., Conticello, V., Egelman, E., Marlovits, T.C., Cheng, Y., and Baker, D. (2015). Atomic-accuracy models from 4.5-A cryo-electron microscopy data with density-guided iterative local refinement. Nat Methods *12*, 361-365.

Egelman, E.H. (2010). Reconstruction of helical filaments and tubes. Methods Enzymol *482*, 167-183.

Emsley, P., and Cowtan, K. (2004). Coot: model-building tools for molecular graphics. Acta Crystallogr D Biol Crystallogr *60*, 2126-2132.

Frank, J., Radermacher, M., Penczek, P., Zhu, J., Li, Y., Ladjadj, M., and Leith, A. (1996). SPIDER and WEB: processing and visualization of images in 3D electron microscopy and related fields. J Struct Biol *116*, 190-199.

Guimaraes, C.P., Witte, M.D., Theile, C.S., Bozkurt, G., Kundrat, L., Blom, A.E., and Ploegh, H.L. (2013). Site-specific C-terminal and internal loop labeling of proteins using sortase-mediated reactions. Nat Protoc *8*, 1787-1799.

Li, X., Mooney, P., Zheng, S., Booth, C.R., Braunfeld, M.B., Gubbens, S., Agard, D.A., and Cheng, Y. (2013). Electron counting and beam-induced motion correction enable near-atomic-resolution single-particle cryo-EM. Nat Methods *10*, 584-590.

McCoy, A.J., Grosse-Kunstleve, R.W., Adams, P.D., Winn, M.D., Storoni, L.C., and Read, R.J. (2007). Phaser crystallographic software J Appl Cryst *40*, 658-674.

Mindell, J.A., and Grigorieff, N. (2003). Accurate determination of local defocus and specimen tilt in electron microscopy. J Struct Biol *142*, 334-347.

Ohi, M., Li, Y., Cheng, Y., and Walz, T. (2004). Negative Staining and Image Classification - Powerful Tools in Modern Electron Microscopy. Biol Proced Online *6*, 23-34.

Otwinowski, Z., and Minor, W. (1997). Processing of X-ray diffraction data collected in oscillation mode. Methods Enzymol *276*, 307-326.

Pettersen, E.F., Goddard, T.D., Huang, C.C., Couch, G.S., Greenblatt, D.M., Meng, E.C., and Ferrin, T.E. (2004). UCSF Chimera--a visualization system for exploratory research and analysis. J Comput Chem *25*, 1605-1612.

Ramaswamy, M., Cruz, A.C., Cleland, S.Y., Deng, M., Price, S., Rao, V.K., and Siegel, R.M. (2011). Specific elimination of effector memory CD4+ T cells due to enhanced Fas signaling complex formation and association with lipid raft microdomains. Cell Death Differ *18*, 712-720.

Sester, D.P., Zamoshnikova, A., Thygesen, S.J., Vajjhala, P.R., Cridland, S.O., Schroder, K., and Stacey, K.J. (2016). Assessment of inflammasome formation by flow cytometry. Current Protocols in Immunology *In Press*.

Tang, G., Peng, L., Baldwin, P.R., Mann, D.S., Jiang, W., Rees, I., and Ludtke, S.J. (2007). EMAN2: an extensible image processing suite for electron microscopy. J Struct Biol *157*, 38-46.